favorable equilibrium with the atmospheric reservoir. Formation of a hydrate is but one component of the ocean disposal process, and it can have a dramatic effect.

References and Notes

1. W. S. Broecker, *Science* **278**, 1582 (1997); C. Hanisch, *Environ. Sci. Technol.* **32**, 20A (1998); E. A. Parson and D. W. Keith, *Science* **282**, 1053 (1998).
2. J. T. Houghton *et al.*, *Climate Change: The IPCC Scientific Assessment* (Intergovernmental Panel on Climate Change, Cambridge Univ. Press, Cambridge, UK, 1990).
3. P. G. Brewer, *Geophys. Res. Lett.* **24**, 1367 (1997); C. Goyet *et al.*, *J. Mar. Res.* **57**, 135 (1999).
4. For injections at depths of <1000 m we used the R/V *Point Lobos* and ROV *Ventana*. The 3627-m experiment was carried out using the R/V *Western Flyer* and the ROV *Tiburon*. The R/V *Western Flyer* is a 35.7-m SWATH (small waterplane area twin hull) ship with a center "moon pool" for ROV deployment. *Tiburon* is a 4000-m capable ROV attached to the mother ship by an armored steel cable with both copper power conductors and single-mode optical fibers for communication and control. Six 3.7-kW electric thrusters supply thrust. The vertical ascent speed is 100 feet/min (30.48 m/min). The experiments were imaged by the vehicle cameras and data were recorded on videotape. The *Ventana* observations were made with a Sony DXC-3000 three-chip camera, and the *Tiburon* made observations with two Panasonic VW E5550 three-chip cameras, with data recorded in digital beta format. Ocean temperature, pressure, and conductivity were sensed continually by a CTD package (Falmouth Scientific) attached to either vehicle within 2 m of the experimental chambers.
5. P. G. Brewer, F. M. Orr Jr., G. Friederich, K. A Kvenvolden, D. L. Orange, *Energy Fuels* **12**, 183 (1998).
6. G. D. Holder, A. V. Cugini, R. P. Warzinski, *Environ. Sci. Technol.* **28**, 276 (1975); I. Aya, K. Yamane, H. Nariai, *Energy* **22**, 263 (1997).
7. K. H. Cole, G. R. Stegen, D. Spencer, *Energy Convers. Manage.* **34**, 991 (1993); D. Archer, H. Kheshgi, E. Maier-Reimer, *Geophys. Res. Lett.* **24**, 405 (1997).
8. E. D. Sloan Jr., *Clathrate Hydrates of Natural Gases* (Dekker, New York, 1990).
9. W. J. North, V. R. Blackwell, J. J. Morgan, *Environ. Sci. Technol.* **32**, 676 (1998).
10. Liquid CO_2 injections were carried out by expulsion from a reservoir by a piston, activated on command from the vehicle control room. For the shallow releases a small volume (~500 ml) steel cylinder was used. For the 3627-m experiment about 9 liters of liquid CO_2 was contained in a commercial accumulator (Parker A4N0578D1) installed horizontally in the tool sled frame. The accumulator was connected to a set of valves and fittings, which permitted loading of the cylinder with liquid CO_2 from standard gas cylinders before the dive. Procedurally, after the first filling, an accumulator gauge pressure of about 600 pounds per square inch (psi) was observed, with the piston set at maximum accumulator capacity. The gas delivery cylinder was then warmed (to compensate for expansion cooling on CO_2 transfer), and the accumulator was packed in ice to lower the temperature of the contained CO_2. A second filling was carried out, and the ice was removed. The filled accumulator was vented to about 750 psi as it warmed to room temperature to prevent overpressure. The system was configured to permit open contact between seawater and the ocean side of the accumulator piston. As the vehicle dived, and pressure increased, the decrease in volume of the contained liquid CO_2 was compensated for by active piston motion to maintain pressure equality. Camera inspection of the pressure gauge during the dive showed the expected drop in accumulator pressure as the pressure-temperature boundary for liquid CO_2 was approached (in practice at a depth of about 400 m), and the differential pressure across the piston dropped effectively to zero. A system check was carried out by opening the quarter-turn CO_2 release valve at several depths during deployment, thereby venting small amounts of liquid CO_2.
11. *Third International Conference on Carbon Dioxide Removal* [Cambridge, MA, Sept. 1996, supplement to *Energy Conversion and Management* **38** (1997)]; R. Socolow, Ed., *Fuels Decarbonization and Carbon Sequestration* (Princeton University CEES Report No. 302, 1997) (www.princeton.edu/~ceesdoe).
12. W. J. Harrison, R. F. Wendtland, E. D. Sloan Jr., *Appl. Geochem.* **10**, 461 (1995).
13. Images of the overflow events are posted along with other supplementary material at www.sciencemag.org/feature/data/987369.shl and at the Monterey Bay Aquarium Research Institute (MBARI) Web site www.mbari.org/ghgases/deep/release.htm
14. H. Sakai *et al.*, *Science* **248**, 1093 (1990).
15. R. Ohmura and Y. H. Mori, *Environ. Sci. Technol.* **32**, 1120 (1998).
16. Y. Fujioka, K. Takeuchi, M. Ozaki, Y. Shindo, H. Komiyama, *Int. J. Energy Res.* **19**, 659 (1995).
17. The total volume of the glass tube was ~7.22 liters (diameter, 30 × 17.5 cm) and the initial volume of liquid CO_2 was 1.8 liters. It is possible to calculate the minimum rate of water incorporation, assuming that the rate of filling [(7.2 liters − 1.8 liters)/4.5 hours = 1.2 liters/hour] was equivalent to hydrate formation, hydrate density was 1.1 kg/liter, and water accounted for 71% of the mass of the hydrate ($CO_2 \cdot 6H_2O$): rate = 1.2 liters/hour × 1.1 kg/liter × 0.71 = 0.94 kg/hour. The actual rate is somewhat faster as some CO_2 is incorporated into the hydrate.
18. K. Ohgaki, Y. Makihara, K. Takano, *J. Chem. Eng. Jpn.* **26**, 558 (1993).
19. R. J. Bakker, J. Dubessy, M. Cathelineau, *Geochim. Cosmochim. Acta* **60**, 1657 (1996).

20. Supported by a grant to MBARI from the David and Lucile Packard Foundation. We thank the MBARI engineers, ROV pilots, and ships' crews for their skilled support.

29 December 1998; accepted 6 April 1999

Spectroscopic Determination of the Water Pair Potential

R. S. Fellers,[1] C. Leforestier,[2] L. B. Braly,[1] M. G. Brown,[1] R. J. Saykally[1]*

A polarizable water pair potential was determined by fitting a potential form to microwave, terahertz, and mid-infrared $(D_2O)_2$ spectra through a rigorous calculation of the water dimer eigenstates. It accurately reproduces most ground state vibration-rotation-tunneling spectra and yields excellent second viral coefficients. The calculated dimer structure and dipole moment are very close to those determined from microwave spectroscopy and high-level ab initio calculations. The dimer binding energy and acceptor switching and donor-acceptor interchange tunneling barriers are in excellent agreement with recent ab initio theory, as are cyclic water trimer and tetramer structures and binding energies.

Much experimental and theoretical effort has been directed toward understanding the nature of the water dimer: the archetype for aqueous hydrogen bonding. Although the dimer structure and hydrogen bond rearrangement dynamics are now fairly well characterized, the equilibrium binding energy (D_e) and dissociation energy (D_0) remain controversial, and these are crucial for properly assessing recently proposed dimer effects in atmospheric chemistry (*1*). Water dimer properties are most succinctly and profoundly expressed in the intermolecular potential energy surface (IPS)—the water pair potential. This pair potential is likewise essential for modeling the condensed phases of water, because it is the principal component of the force field (three- and four-body interactions are much weaker). The water pair potential has heretofore eluded accurate determination because of technological and computational impediments. Here we describe the determination of a polarizable water pair potential by regression analysis of the rotational constants, tunneling splittings, and intermolecular vibrational frequencies precisely determined from microwave, terahertz, and infrared vibration-rotation-tunneling (VRT) spectroscopy of the water dimer (*2, 3*). Our previous experience with simpler IPS determinations indicates that such measurements provide an exacting measure of the relevant force field (*4*).

Theoretical and spectroscopic studies have shown that the six-dimensional (6D) water IPS has a complex topology. There are eight identical global minima, differing only by permutations of the four hydrogen atoms and two oxygens that do not break covalent bonds [the permutation-inversion symmetry group is $D_{4h}(M)$]. Ab initio calculations (*5*) have revealed three low-energy paths connecting these eight degenerate minima: "acceptor switching" (equivalent to a 180° rotation of the hydrogen bond acceptor about its symmetry axis), "interchange" (exchange of the role of donor and acceptor of the hydrogen bond), and "bifurcation" (exchange of bound and free hydrogens

[1]Department of Chemistry, University of California, Berkeley, CA 94720–1460, USA. [2]Laboratoire Structure et Dynamique des Systèmes Moléculaires et Solides (UMR 5636), CC 014, Université des Sciences et Techniques du Langue-doc, 34095 Montpellier Cédex 05, France.

*To whom correspondence should be addressed. E-mail: saykally@uclink4.berkeley.edu

on the donor). The associated barrier heights are given in Table 1. The water monomers rearrange their hydrogen bonding orientations through quantum tunneling among these eight minima, much like the familiar umbrella inversion tunneling in the NH_3 molecule. This effects a splitting of each dimer rovibrational level into a manifold of either 6 or 10 tunneling states (Fig. 1), where the E states are doubly degenerate. These splittings can be measured precisely (~1 MHz) by high-resolution spectroscopy.

The IPS used here is the highly detailed ASP-W distributed multipole form of Millot and Stone (*6*), in which each intermolecular interaction (electrostatics, induction, dispersion, and exchange) is treated separately. The 72 parameters of this potential were originally determined by a combination of experiment and ab initio calculations. As in the original ASP-W paper, we compute the iterated induction to first order, resulting in a small but acceptable error in the induction energy and a significant reduction in computation time as compared to computing the induction to full convergence. The explicit potential form and parameter sets are available from the authors (*7*).

The observables in the nonlinear least-squares regression analysis are the spectroscopically determined tunneling levels of $(D_2O)_2$ in the lowest two rotational states (J = 0 and J = 1) of the ground vibrational state and in J = 0 of the excited intermolecular vibrational states near 68, 83 (*8*), and 104 cm^{-1}. Only $(D_2O)_2$ data are used, because the corresponding $(H_2O)_2$ spectra have many more unobservable VRT states due to unfavorable nuclear spin statistics, making it difficult to determine the bifurcation or interchange splittings. In contrast, these splittings are completely determined for $(D_2O)_2$. Moreover, recent infrared cavity ringdown experiments by Paul *et al.* (*9*) have determined the $(D_2O)_2$ ground state acceptor tunneling splitting, whereas this has not been possible to do for $(H_2O)_2$. However, by scaling the fitted potential for $(D_2O)_2$ mass effects, the corresponding properties for $(H_2O)_2$ can be calculated.

The computationally demanding calculation of VRT states on the 6D IPS that is required for regression analysis was made possible by use of the recently developed Split Wigner Pseudo Spectral (SWPS) algorithm (*10, 11*), which accurately and efficiently yields the eigenstates within a scattering theory formalism. Only a subset of the available data was used in the fit, in order to make this very large calculation feasible (13 microwave transitions and tunneling splittings of the J = 0 and J = 1 ground state and 8 J = 0 terahertz transitions in the three observed vibrational bands).

With judicious selection of these data, we could avoid calculating half of the A/B states and all of the E states (Fig. 1). The latter is crucial because the doubly degenerate E states require twice as many basis functions and three times the computer processing time for convergence. This truncation does not generally affect the results of the fit, because the spectroscopic data are so highly redundant (that is, not independent), but it did preclude a direct fit of the small ($\sim 3 \times 10^{-4}$ cm^{-1}) bifurcation shifts. The basis set for these calculations employed the minimum set of functions that converged the J = 0 inter-

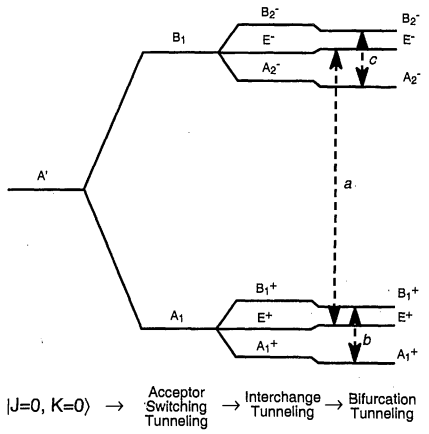

Fig. 1. The effect of the three tunneling motions on the lowest energy water dimer rovibrational state with labeled splittings. The symmetry labeling scheme is determined from permutation inversion group theory (*2*). These labels describe the symmetry of the different water dimer tunneling wave functions. The splitting or shift of the VRT states is inversely related to the tunneling barriers. Acceptor switching, which has the smallest barrier, causes each rovibrational state to be split into two: A_1 and B_1 (splitting denoted by *a*). Interchange tunneling further splits each of those states into three (splitting denoted by *b* and *c*). Bifurcation tunneling, which has the highest barrier, causes a small shift of the $E^{-/+}$ states but does not cause further splitting, because the first two motions have already resolved all the available states.

Table 1. A comparison of the ground state properties of $(D_2O)_2$ and tunneling barriers of the IPS. Numbers in parentheses indicate the error in the last digit; dashes indicate that the information is not available.

	Ground state water dimer properties				
	Experimental*	VRT (ASP-W)$_{vib}$†	VRT (ASP-W)$_{eq}$†	Ab initio‡	ASP-W§
D_e (kcal/mol)	5.40 (0.5)	–	4.91	5.05	4.69
D_0 (kcal/mol)	3.66 (0.5)	3.46	–	–	–
R_{OO} (Å)	2.976 (0.00–0.03)	2.94 (3)	2.924	2.953	2.972
θ_a (deg.)	57 (10)	41 (2)	48.5	56.0	64.6
θ_d (deg.)	51 (10)	58 (2)	50.2	59.1	44.5
A (GHz)	124.9	123.7	115.6	–	–
$(B + C)/2$ (GHz)	5.433	5.423	5.570	–	–
$B - C$ (MHz)	33.11	30.79	14.94	–	–
μ_a (Debye)	2.60	2.65 (10)	2.69 (10)	–	–

	Tunneling barriers (cm^{-1})			
	VRT (ASP-W)	Ab initio‖	Ab initio¶	ASP-W
Switching (cm^{-1})	157	158	175	277
Interchange (cm^{-1})	207	199	204	149
Bifurcation (cm^{-1})	394	612	476	484

*The B and C rotational constants and dipole moment were measured by microwave and Stark experiments of Odutola and Dyke (*27*). Using these data in conjunction with measurements for other dimer isotopes, they derived the equilibrium structure parameters R_{OO}, θ_d, and θ_a using a constrained model (rigid monomers). The structure parameters are defined in Fig. 2. The A rotation constant is estimated from the far-infrared measurements of Karyakin *et al.* (*28*). The equilibrium and zero-point dissociation energies are from the thermal conductivity experiments of Curtiss et al. (*13*). †The VRT (ASP-W) vibrationally averaged structure was determined by the DQMC method. The rotational constants were calculated using fixed monomer geometries of ∠HOH = 104.52° and R_{OH} = 0.9572 Å and masses D = 2.0141022 and O = 15.994915. Note the excellent agreement between the experimental observables A, $(B + C)/2$, $B - C$, and μ_a (dipole moment projected on the principal axis), which are model-independent, and the vibrationally averaged values predicted by VRT (ASP-W). ‡High level ab initio calculations of Mas and Szalewicz using symmetry-adapted perturbation theory (*16*). §The original ASP-W potential of Millot and Stone (*6*). The principal tunneling barriers of the VRT (ASP-W) and ASP-W surfaces are compared to ab initio results of ‖Smith *et al.* (*5*) and ¶Wales (*23*). The VRT (ASP-W) and ASP-W barriers were found with the Orient program (*29*). Ab initio calculations were performed at the MP2 level with counterpoise corrections to improve accuracy.

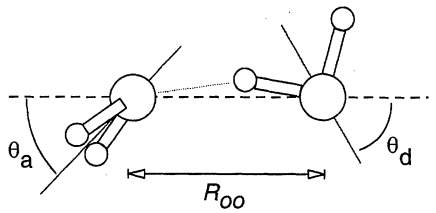

Fig. 2. The water dimer. R_{OO}, center-of-mass separation between the two monomers; θ_a, angle made by the acceptor monomer symmetry axis with R_{OO}; θ_d, angle made by the donor monomer symmetry axis with R_{OO}.

change and acceptor switching splittings to better than 0.02 cm^{-1} in the ground state. Typically, a single iteration of the fit required 12 to 20 computing hours on an IBM RS/6000 590 workstation. The total computational effort required about 6 months of computing time.

After exploring the sensitivity of the data to the parameters in ASP-W, we concluded that changing the exchange-repulsion terms had the largest effect on the spectra, which is consistent with the findings in our previous Ar–H_2O, Ar–NH_3, and $(HCl)_2$ IPS determinations (*4, 12*). Ultimately, eight of the exchange-repulsion parameters describing this interaction were varied in the fit. The final fitted values, compared with original ASP-W parameters, are also available (*7*).

The quality of the fitted IPS, which we call VRT (ASP-W), was assessed in several ways. Table 1 shows the excellent agreement of the VRT (ASP-W) ground state water dimer structure (Fig. 2) and dipole moment with experimental and ab initio results, and that they are much improved relative to ASP-W. The fitted potential was also used to predict VRT states up to total angular momentum J = 2 not explicitly included in the fit, yielding excellent agreement (largest error = 0.16 cm^{-1}, or <1% of transition frequency, with most errors being an order of magnitude smaller). For the excited VRT states near 68, 83, and 104 cm^{-1}, the agreement with experimental results is not as good (~1 to 5 cm^{-1}), but it is nevertheless clear from Fig. 3 that VRT (ASP-W) reproduces the energy-level spectrum of the water dimer very well, and this is a most demanding test of a potential surface. For comparison, we have computed these VRT states on a number of other potentials (*11*) (including TIP4P; SPC; MCY; and polarizable SPC, RWK2, NEMO3, TIP-FQ, ASP-S, and ASP-W) and have found that all produce energy-level patterns that deviate significantly from experimental results, as shown for the original ASP-W, previously considered to be the best dimer IPS.

One of the most important properties of the water dimer is the binding energy (D_e). The most often quoted experimental value is 5.4 ± 0.7 kcal/mol, derived from the dissociation energy measured in thermal conductivity experiments (*13*). Reimers et al. (*14*) recommended the same value for D_e with tighter error bars (5.4 ± 0.2 kcal/mol). This value is too large because it is obtained with the use of crude harmonic ab initio vibrational frequencies. Ab initio calculations of D_e have given values ranging from 5.6 to 4.6 kcal/mol, although the most recent and sophisticated calculations converge to a value of 5.0 ± 0.1 kcal/mol (*15–18*). Our VRT (ASP-W) potential gives D_e = 4.91 kcal/mol. Using diffusion quantum Monte Carlo (DQMC) methods (*19*) to perform the requisite vibrational averaging, we have also calculated the $(D_2O)_2$ dissociation energy (D_0) of the ground state as 3.46 kcal/mole, which compares well with experimental results (Table 1).

Second viral coefficients (SVCs)—coefficients of the squared density in the power series expansion of the equation of state *P/RT* for a vapor—are a time-honored measure of a pair potential (*20*). Comparison of the temperature dependence of SVCs calculated from VRT (ASP-W) with experimental values obtained from H_2O and D_2O steam measurements (*21*) shown in Fig. 4 constitutes a stringent test of the overall validity of our potential, because SVCs are sensitive to both the attractive well depth and the angle-averaged potential (*22*). Essentially perfect agreement is found for both H_2O and D_2O isoto-

Table 2. Geometrical parameters and energies for the water trimer and tetramer cyclic ground state. Pairwise and iterated *n*-body induction forces for VRT (ASP-W) and ASP-W are calculated to the first order. Vibrationally averaged structures and energies are computed by the DQMC method. D_e and D_0 specify the energy required to break all hydrogen bonds. Distances are in angstroms and energies are in kilocalories per mole. Dashes indicate that the information is not available.

	Experimental*	VRT (ASP-W)	ASP-W	TIP4P†	Ab initio‡
		Trimer			
Avg. $R_{OO(eq)}$	–	2.756	2.881	2.764	2.799
Avg. $R_{OO(vib)}$	2.845	2.843	–	–	–
D_e	–	15.65	14.82	16.73	14.05
D_0	–	11.11	–	–	–
		Tetramer			
Avg. $R_{OO(eq)}$	–	2.783	2.866	2.730	2.743
Avg. $R_{OO(vib)}$	2.789	2.838	–	–	–
D_e	–	25.93	24.33	27.87	24.33
D_0	–	19.33	–	–	–

*(*30*). †(*31*). ‡MP2/aug-cc-pVDZ with counterpoise correction (*18*).

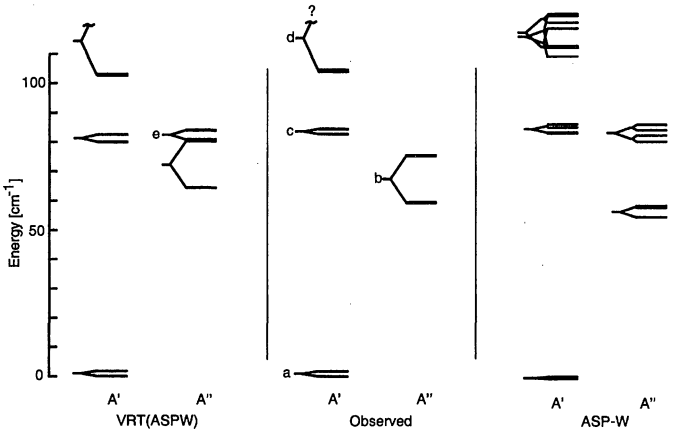

Fig. 3. The ordering of the J = 0 VRT states below 110 cm^{-1} of $(D_2O)_2$ calculated with the VRT (ASP-W) and ASP-W potentials are compared to measured J = 0 states. Shown are the upper and lower A/E/B interchange triplets segregated by A′ or A″ vibrational symmetry (Fig. 1). On the scale of this plot, the individual interchange triplets are only partially resolvable; therefore, the symmetry labels for individual levels have been omitted for clarity. The A′ and A″ labels denote vibrations that are symmetric and antisymmetric with respect to the plane of symmetry, respectively. Note the excellent agreement of the tunneling splittings and positions of the vibrational bands. a, the ground state levels assigned by microwave spectroscopy; b, the 68 cm^{-1} band; c, the 83 cm^{-1} band; d, the 104 cm^{-1} band, where only states associated with the lower interchange triplet have been observed. The upper interchange triplet is predicted to be at least 10 cm^{-1} higher in energy. e: Motivated by predictions of this band, one of us (L.B.B.) has recently reanalyzed the 83 cm^{-1} band data set and has discovered an A″ band centered around 90 cm^{-1}. This new band is not plotted in the observed category as the tunneling splittings of this new band have not yet been determined.

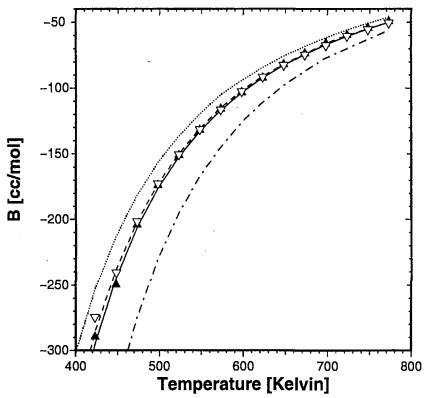

Fig. 4. The temperature-dependent SVCs of VRT (ASP-W) with D_2O (solid line) and H_2O (dashed line), ASP-W with H_2O (dotted line), TIP4P with H_2O (dash-dotted line), and the H_2O (open triangles) and D_2O (solid triangles) experimental data of Kell *et al.* (*21*). B, the SVC, is the deviation of the density of steam from the idea gas law. This deviation is a direct manifestation of pairwise interactions in the gas.

pomers, representing a significant improvement over the original ASP-W results (which were already fairly good).

From Table 1 we find very good agreement between the two lowest tunneling barriers on VRT (ASP-W) and ab initio calculations (*5, 23*), indicating that the topological features of the 6D IPS are adequately represented. The highest barrier (for bifurcation), which is not explicitly constrained in the fit, may be too small on VRT (ASP-W), but it is difficult to ascertain this given the large variations in ab initio values. In general, we clearly see significant improvements in the barrier heights relative to those on the ASP-W surface, indicating that the hydrogen bond rearrangement dynamics in the dimer will be properly represented.

To further characterize VRT (ASP-W), we have computed both equilibrium and vibrationally averaged ground state structures, D_e, and D_0 for cyclic D_2O trimers and tetramers, which have been characterized by terahertz laser spectroscopy (*3*). This was done using DQMC on a trimer (tetramer) IPS constructed by pairwise addition of the pair potentials, followed by computing first-order, iterated, *n*-body induction. As shown in Table 2, good agreement is found with both ab initio and experimental results, and again a significant improvement relative to ASP-W is found, which generally produced O–O distances that were too long. Effective pair potentials, such as TIP4P, are not able to reproduce the cluster features, yielding rather short O–O distances and binding energies that are too large. That a pair potential such as VRT (ASP-W) does so well in calculating properties of larger clusters is not entirely unexpected, as the dominant *n*-body force is induction (polarization), which is explicitly treated by the polarizable VRT (ASP-W) potential. In contrast, effective pair potentials parameterize the many-body forces in an average way according to bulk properties and so are unable to simultaneously describe both small clusters and the bulk.

The principal weakness in the VRT (ASP-W) potential is the constraint of frozen water monomers to equilibrium properties. It is known that the donor O-H bond actually elongates slightly (<1%) upon hydrogen bond formation, accompanied by smaller changes in the bond angle (*24, 25*). Although these subtle effects must eventually be included to obtain a "perfect" water pair potential, to do so requires a complete 12D treatment of the VRT dynamics and potential surface, which currently transcends the state of the art. Preliminary explorations indicate that the main effects of including monomer nonrigidity involve some reduction in the acceptor switching splitting and a small (~0.1 kcal/mol) increase in D_e. In any case, we expect the effects of monomer nonrigidity on the fitted potential to be relatively minor (*25*); VRT (ASP-W) is clearly quite close to the "exact" water pair potential. Moreover, as computational power continues to increase, it will ultimately become possible to determine the small exchange-repulsion and dispersion contributions to the many-body interactions (*26*) that are operative within aggregates of water molecules, as well as to further refine subtle features of the pair potential by comparing results computed rigorously from this pair potential with the precise VRT data measured for the water trimer, tetramer, pentamer, and hexamer. Hence, a truly rigorous molecular description of the force fields of solid and liquid water seems close at hand.

References and Notes

1. S. Solomon, R. W. Portman, R. W. Sanders, J. S. Daniel, *J. Geophys. Res.* **103**, 3847 (1998).
2. G. T. Fraser, *Int. Rev. Phys. Chem.* **10**, 189 (1991).
3. K. Liu, J. D. Cruzan, R. J. Saykally, *Science* **271**, 929 (1996) and references therein.
4. R. J. Saykally and G. A. Blake, *ibid.* **259**, 1570 (1993).
5. B. J. Smith, D. J. Swanton, J. A. Pople, H. F. Schaefer, L. Radom, *J. Chem. Phys.* **92**, 1240 (1990).
6. C. Millot and A. J. Stone, *Mol. Phys.* **77**, 439 (1992).
7. The potential form and parameter sets are available at www.cchem.berkeley.edu/~rjsgrp/.
8. N. Pugliano and R. J. Saykally, *J. Chem. Phys.* **96**, 1832 (1992).
9. J. B. Paul, R. A. Provencal, R. J. Saykally, *J. Phys. Chem. A* **102**, 3279 (1998).
10. C. Leforestier, L. B. Braly, K. Liu, M. J. Elrod, R. J. Saykally, *J. Chem. Phys.* **106**, 8527 (1997).
11. R. S. Fellers, L. B. Braly, R. J. Saykally, C. Leforestier, *ibid.* **110**, 6306 (1999).
12. M. J. Elrod and R. J. Saykally, *ibid.* **103**, 933 (1995).
13. L. A. Curtiss, D. J. Frurip, M. Blander, *ibid.* **71**, 2703 (1979).
14. J. R. Reimers, R. O. Watts, M. L. Klein, *Chem. Phys.* **64**, 95 (1982).
15. M. W. Feyereisen, D. Feller, D. A. Dixon, *J. Phys. Chem.* **100**, 2993 (1996).
16. E. M. Mas and K. Szalewicz, *J. Chem. Phys.* **104**, 7606 (1996).
17. A. Halkier *et al.*, *Theor. Chem. Acc.* **97**, 150 (1997).
18. S. S. Xantheas, *J. Chem. Phys.* **110**, 4566 (1999) and references therein.
19. J. K. Gregory and D. C. Clary, *ibid.* **102**, 7817 (1995).
20. D. A. McQuarrie, in *Statistical Mechanics*, S. A. Rice, Ed. (Harper and Row, New York, 1976).
21. G. S. Kell, G. E. McLaurin, E. Whalley, *Proc. R. Soc. London Ser. A* **425**, 49 (1989).
22. C. Millot, J. C. Soetens, M. T. C. Martins-Costa, M. P. Hodges, A. J. Stone, *J. Phys. Chem. A* **102**, 754 (1998).
23. D. J. Wales, in *Theory of Atomic and Molecular Clusters 2*, J. Jellick, Ed. (Springer-Verlag, Heidelberg, Germany, in press) (see http://brian.ch.cam.ac.uk/publications.html).
24. S. Xantheas and T. H. Dunning, *J. Chem. Phys.* **99**, 8774 (1993).
25. J. K. Gregory and D. C. Clary, *J. Phys. Chem.* **100**, 18014 (1998).
26. M. J. Elrod and R. J. Saykally, *Chem. Rev.* **94**, 1975 (1994).
27. J. A. Odutola and T. R. Dyke, *J. Chem. Phys.* **72**, 5062 (1980).
28. E. N. Karyakin, G. T. Fraser, R. D. Suenram, *Mol. Phys.* **78**, 1179 (1993).
29. A. J. Stone, A. Dullweber, P. L. A. Popelier, D. J. Wales, *Orient: A Program for Studying Interactions Between Molecules, Version 3.2* (University of Cambridge, Cambridge, 1995), available at http://fandango.ch.cam.ac.uk/.
30. K. Liu, M. G. Brown, R. J. Saykally, *J. Phys. Chem. A* **101**, 8995 (1997).
31. W. L. Jorgensen, J. Chandrasekhar, J. D. Madura, R. W. Impey, M. L. Klein, *J. Chem. Phys.* **79**, 926 (1983).

32. We thank C. Millot and A. Stone for providing the source code of the ASP-W potential. Supported by the Experimental Physical Chemistry Program of NSF and the France-Berkeley Cooperative Grant Program.

22 December 1998; accepted 22 March 1999

Design and Self-Assembly of Open, Regular, 3D Mesostructures

Tricia L. Breen, Joe Tien, Scott R. J. Oliver, Tanja Hadzic, George M. Whitesides*

Self-assembly provides the basis for a procedure used to organize millimeter-scale objects into regular, three-dimensional arrays ("crystals") with open structures. The individual components are designed and fabricated of polyurethane by molding; selected faces are coated with a thin film of liquid, metallic alloy. Under mild agitation in warm, aqueous potassium bromide solution, capillary forces between the films of alloy cause self-assembly. The structures of the resulting, self-assembled arrays are determined by structural features of the component parts: the three-dimensional shape of the components, the pattern of alloy on their surfaces, and the shape of the alloy-coated surfaces. Self-assembly of appropriately designed chiral pieces generates helices.

We describe a procedure that uses self-assembly of patterned, three-dimensional (3D), mesoscale (millimeter- to centimeter-scale) objects to generate open, regular, 3D structures. These types of structures may eventually find use as the cores of densely interconnected, 3D electronic and optical elements for high-performance computation and sensors. We prepared millimeter-scale objects (both polyhedra and more complex shapes designed to form an extended lattice), coated selected faces with a film

Department of Chemistry and Chemical Biology, Harvard University, 12 Oxford Street, Cambridge, MA 02138, USA.

*To whom correspondence should be addressed.